Received: 25 March 2022 | Revised: 6 May 2022 | Accepted: 24 May 2022

DOI: 10.1002/oby.23519

ORIGINAL ARTICLE

Obesity Biology and Integrated Physiology

Obesity A Research Journal | THE OBESITY SOCIETY | WILEY

Xenon-enhanced computed tomography assessment of brown adipose tissue distribution and perfusion in lean, obese, and diabetic primates

John C. Garside[1,2] | Kylie Kavanagh[3,4] | Masha R. Block[3] | Abigail G. Williams[3] | Rosa T. Branca[1,2]

[1]Department of Physics and Astronomy, University of North Carolina at Chapel Hill, Chapel Hill, North Carolina, USA

[2]Biomedical Research Imaging Center, University of North Carolina at Chapel Hill, Chapel Hill, North Carolina, USA

[3]Department of Pathology, Wake Forest University School of Medicine, Winston-Salem, North Carolina, USA

[4]College of Health and Medicine, University of Tasmania, Hobart, Tasmania, Australia

Correspondence
Rosa T. Branca, Department of Physics and Astronomy, University of North Carolina at Chapel Hill, 27599 Chapel Hill, North Carolina, USA.
Email: rtbranca@unc.edu

Funding information
National Institute of Diabetes and Digestive and Kidney Diseases, Grant/Award Numbers: R01DK108231, R01DK123206; National Institutes of Health, Grant/Award Numbers: P40OD010954, P40OD010965, R01HL142930, ULTR001420; U.S. Department of Defense, Grant/Award Numbers: W81XWH-1510574, W81XWH-2110565

Abstract

Objective: This study aimed to validate xenon-enhanced computed tomography (XECT) for the detection of brown adipose tissue (BAT) and to use XECT to assess differences in BAT distribution and perfusion between lean, obese, and diabetic non-human primates (NHPs).

Methods: Whole-body XECT imaging was performed in anesthetized rhesus and vervet monkeys during adrenergic stimulation of BAT thermogenesis. In XECT images, BAT was identified as fat tissue that, during xenon inhalation, underwent significant radiodensity enhancement compared with subcutaneous fat. To measure BAT blood flow, BAT radiodensity enhancement was measured over time on the six computed tomography scans acquired during xenon inhalation. Postmortem immunohistochemical staining was used to confirm imaging findings.

Results: XECT was able to correctly identify all BAT depots that were confirmed at necropsy, enabling construction of the first comprehensive anatomical map of BAT in NHPs. A significant decrease in BAT perfusion was found in diabetic animals compared with obese animals and healthy animals, as well as absence of axillary BAT and significant reduction of supraclavicular BAT in diabetic animals compared with obese and lean animals.

Conclusions: The use of XECT in NHP models of obesity and diabetes allows the analysis of the impact of metabolic status on BAT mass and perfusion.

INTRODUCTION

BAT expends energy through nonshivering thermogenesis (NST), a process in which uncoupling protein 1 (UCP1) short-circuits the inner mitochondrial membrane [1–4]. UCP1 uncouples the proton gradient produced by the electron transport chain that is typically used for the synthesis of ATP, allowing protons to flow down their gradient while dissipating energy as heat [1–4].

Although NST by BAT may be an attractive mechanism for increasing energy expenditure to combat excess energy intake as dietary calories and resultant obesity, the total mass and precise locations of BAT in humans are largely unknown. Consequently, the

contribution of BAT to daily energy expenditure is still a topic of debate. To assess the effect of BAT on metabolism in patients with obesity, in whom BAT could be a target for novel antiobesity drugs, there must be an accurate noninvasive imaging technique to quantify BAT mass and activity. To date, there remains no proven imaging method for precise identification of BAT and its activity *in vivo* in humans [5–7].

Positron emission tomography with fluorodeoxyglucose (^{18}F-FDG-PET) is what originally led to the discovery of BAT. While the method has taught us a great deal about this tissue since then [8], its reliance on glucose uptake prevents accurate anatomical mapping of BAT in the general population, especially in subjects with obesity and diabetes [9, 10]. Indeed, glucose uptake in BAT is influenced by factors including blood glucose and insulin levels, feeding status, and cold adaptation and, in general, is not directly associated with heat production [9, 10]. As a result, a wide range of conclusions about BAT distribution is inevitable when quantifying this tissue with ^{18}F-FDG standardized uptake values [11, 12]. Additionally, although ^{18}F-FDG-PET has suggested that BAT activity is significantly lower in patients with obesity compared with lean patients [13], the dissociation between BAT activity and glucose uptake has demonstrated that these results may not be reliable [9, 10, 14]. Computed tomography (CT) and magnetic resonance imaging have also been explored as a method of locating and quantifying BAT [15, 16], but their results depend on BAT hydration [17]. It has been shown that, unlike in rodents, human BAT can be difficult to differentiate from white adipose tissue (WAT), as this tissue is not found in large quantities and is often found interspersed within WAT, especially in subjects with obesity [18, 19].

The nonradioactive and lipophilic gas xenon is a viable CT contrast agent for detecting BAT [19]. Because of its high atomic number, xenon causes efficient attenuation of the x-ray radiation. Thanks to its radiodensity properties and relatively high solubility in tissues, xenon-enhanced CT (XECT) has been historically used in humans to quantify not only lung ventilation but also brain perfusion [20–22]. Tissue enhancement is directly proportional to the concentration of xenon in the tissue and measurements of radiodensity enhancement during xenon inhalation can provide a direct and accurate way to quantify tissue perfusion [23–25]. In previous XECT studies, a localized increase in BAT radiodensity was shown in lean and obese mouse phenotypes as well as in healthy lean nonhuman primates (NHPs) during xenon inhalation and following adrenergic stimulation of BAT thermogenesis. The enhancement obtained in BAT was observed to be independent of BAT's glucose uptake capacity (measured during the same imaging session) and significantly greater than that of WAT and muscle [26]. This specific enhancement in BAT radiodensity during xenon inhalation was the result of the specific increase in BAT blood flow that has been widely observed in rodents, NHPs, and humans during stimulation of NST [27, 28].

In this study, we first used XECT imaging in NHPs followed by postmortem evaluation of BAT to assess the accuracy of XECT in identifying BAT depots *in vivo*. Then we used XECT to examine how BAT distribution and perfusion compare between healthy lean, obese, and diabetic NHPs. We investigated the occurrence of BAT in different regions of the body and we provide the first comprehensive anatomical map of BAT in NHPs to our knowledge.

The use of NHPs in this study is motivated by their phylogenetic similarity with humans in terms of adipose distributions and progression of obesity and metabolic diseases [29]. In contrast to mice, which tend to have BAT predominantly concentrated in the interscapular region [14, 19, 26], humans and NHPs have very similar anatomical distributions of BAT, with the main depots located in the supraclavicular and axillary regions [30, 31]. Rhesus and vervet monkeys, in particular, spontaneously develop obesity and diabetes as they age at prevalence rates comparable to that of humans [31]. Moreover, in both humans and NHPs, NST in BAT is activated through the same signaling cascade: the binding of catecholamines to adrenergic receptors increases intracellular cyclic AMP, stimulates lipolysis, and consequently upregulates UCP1 in the mitochondria [31, 32]. Taken together, these similarities suggest that NHPs are a valuable model for studying BAT and its implication in the development of obesity and diabetes. Finally, the use of XECT in NHPs enables us to validate this methodology in a way that cannot be done in humans for evident practical and ethical reasons.

Study Importance

What is already known?

- Brown adipose tissue (BAT) is a potential target for antiobesity drugs.
- Xenon is an effective contrast agent for computed tomography, and it has been used previously to detect and quantify BAT in rodents and healthy lean nonhuman primates (NHPs).

What does this study add?

- Significant differences in BAT distribution and perfusion are observed between lean, obese, and diabetic NHPs.
- The axillary depot is generally less perfused than the supraclavicular depot, and it is scarce in obese animals and absent in diabetic animals.

How might these results change the direction of research?

- Our findings demonstrate XECT's ability to noninvasively detect BAT and measure its perfusion in obese and diabetic subjects.
- Temporal changes in BAT mass and perfusion as detected by XECT may be used to understand the relationship between changes in BAT mass and perfusion and the progression of metabolic diseases.

METHODS

Imaging protocol

XECT studies were performed on five male rhesus macaques (*Macaca mulatta*) and eleven female vervet monkeys (*Chlorocebus aethiops sabaeus*), under propofol anesthesia, on a Somatom Definition Flash CT scanner (Siemens Healthineers) in single-energy mode (80 kV). The animals were selected to represent a range of health and obesity states (Table 1; Supporting Information Table S1). The animals were first sedated with an injection of 10 mg/kg of ketamine. Anesthesia was induced with propofol (2 mg/kg intravenous bolus) before orotracheal intubation. Anesthesia was maintained during the entire imaging session with propofol at a dose of 0.15 mg/kg/min via calibrated syringe pump and titrated to maintain immobilization and spontaneous ventilation. For the CT scans, the intratracheal tube was open to air, whereas, for all XECT scans, the intratracheal tube was connected to a closed-circuit xenon rebreathing system (Biodex Medical Systems, Inc.) containing a gas reservoir with 30% volume xenon in oxygen. During xenon inhalation, the xenon rebreathing system was connected to an oxygen source to offset oxygen consumption. In rhesus macaques, an initial CT scan was performed followed by the acquisition of a series of XECT scans. In two of the five subjects, norepinephrine was infused at a rate of 0.4 mg/kg/min during the acquisition of the XECT scans. In all vervet monkeys, an initial CT scan was performed followed by the initiation of norepinephrine infusion, which was administered at a dose of 0.4 mg/kg/min and which lasted until the end of the acquisition of XECT scans, performed every 5 minutes for a total of 25 minutes. Less than a month after the XECT study, the rhesus macaques were euthanized for reasons unrelated to this study. BAT depots were identified at necropsy using XECT image guidance, and tissues were then collected and processed for immunohistochemical staining (Supporting Information Figure S1). Tissue collection protocol and images are provided in the online Supporting Information.

Immunohistochemistry analysis of BAT tissue

Tissues were fixed in 10% neutral buffered formalin for at least 24 hours prior to storage in 70% ethanol until tissues were paraffin embedded for histological sectioning. Four-micron sections were made and stained with hematoxylin and eosin and for UCP1 (Fischer Scientific Cat# PA124894). Stained slides were scanned at 20× magnification and visualized using an optical microscope (OlyVIA, Olympus Corp). Positive and negative controls were established in tissue taken from the axillary region of an African green monkey at necropsy (Supporting Information Figure S2).

BAT quantification

CT images were analyzed using Horos (Nimble Co., LLC d/b/a Purview) by one investigator blinded to the animals' metabolic status. Three-dimensional (3D) contours of BAT were made using the open software package 3D Slicer [33]. Anatomical landmarks were used to guide the identification of BAT in the cervical, supraclavicular, axillary, pericardial, paraspinal, intervertebral, interscapular, and perirenal regions of the NHPs. BAT was identified as tissue with an initial radiodensity, measured in Hounsfield units (HU), between −150 and 50 that also underwent a radiodensity enhancement during xenon inhalation exceeding that of subcutaneous fat by at least three standard deviations [SD].

Measurements of BAT blood flow

XECT has been historically used to measure cerebral blood flow [34–36]. This technique is considered a gold standard for blood flow measurements and is often used to validate other methodologies.

In order to quantify blood flow in BAT using XECT, radiodensity enhancement was measured over time on the six CT scans acquired during xenon inhalation. The time-dependent enhancement seen in

TABLE 1 Phenotypic data of the NHPs imaged by XECT

	Healthy lean	Healthy obese	Unhealthy obese	*p* value
n	3	3	5	—
Age (y)	16.67 (2.33)	14.00 (0.58)	18.80 (1.46)	0.169
Body weight (kg)	4.58 (0.36)	6.38 (0.18)	6.88 (0.58)	0.035
Waist circumference (cm)	31.50 (2.25)	42.33 (1.86)	42.30 (2.52)	0.029
Fat (% BW)	12.12 (5.68)	27.08 (5.04)	26.38 (1.21)	0.041
Fasting glucose (mg/dL)	80.33 (7.53)	86.00 (7.81)	328.40 (62.25)	0.011
A1c (%)	3.90 (0)	3.97 (0.07)	7.84 (1.05)	0.014

Note: Data given as mean (SE). The animals were classified as lean based on computed tomography assessment of total body fatness as a percentage of body weight and waist circumference. Prediabetes and type 2 diabetes were defined by American Diabetes Association criteria for fasting glucose and glycosylated hemoglobin A_{1c} levels. Healthy obese animals were obese but without any evidence of impaired glycemic control.
Abbreviations: A1c, glycosylated hemoglobin A_{1c}; BW, body weight; NHP, nonhuman primate; XECT, xenon-enhanced computed tomography.

each region of interest was then fitted to the Kety–Schmidt equation [23]. Parameters used for the model and examples of dynamic enhancement curves seen in different tissues are provided in Supporting Information Figures S3 and S4.

Statistical analysis

All statistical analysis was performed using JMP (version 16.1.0, SAS Institute, Inc.) software. To compare BAT blood flow, radiodensity (used here as a proxy for tissue's hydration) [37], and mass across different metabolic groups in vervet monkeys, significant differences with $p < 0.05$ were determined using a Tukey–Kramer honestly significant difference (HSD) test for multiple comparisons. A matched-pairs t test was used to assess intrasubject variability of BAT perfusion between the supraclavicular and axillary regions of vervet monkeys.

RESULTS

XECT detection in rhesus monkeys and histological validation

In XECT scans, areas of suspected BAT were identified in the supraclavicular and axillary regions based on tissue radiodensity enhancement. Significant xenon uptake in BAT relative to WAT, as shown in Figures 1 and 3, made the tissue stand out on CT images. Immunohistochemical staining of BAT confirmed the presence of UCP1-positive adipocytes in areas that underwent a significant radiodensity enhancement following xenon inhalation.

Figures 1 to 4 and Supporting Information Figure S5 show representative radiodensity enhancement seen in the supraclavicular, axillary, and renal hila following xenon inhalation, along with the corresponding gross images and immunohistochemical sections of enhanced depots. The healthy lean rhesus presented diffuse BAT in the supraclavicular and axillary regions (Figure 1) that was confirmed through necropsy and immunohistochemistry analysis of the excised tissue (Figure 2). XECT also showed BAT in the renal hilum of the same animal that was also visible at necropsy (Figure 1C; Supporting Information Figure S4A). In Figures 3 and 4, XECT images show BAT in a prediabetic animal. In XECT scans, this animal presented a fairly large amount of BAT in the supraclavicular region but only a very small amount in the axillary region, a finding confirmed by histology (Figure 4; Supporting Information Figure S4B).

The lean rhesus macaque showed a mean radiodensity enhancement of 38 (3) HU in the supraclavicular region and 25 (5) HU in the axillary region. The prediabetic rhesus had a mean radiodensity enhancement of 18 (4) HU in the supraclavicular region and 11 (4) HU in the much smaller BAT depots identified in the axillary region.

Our findings in rhesus macaques foreshadow clear patterns that became much more evident as we studied the larger sample size of vervet monkeys (BAT is significantly more perfused in healthy NHPs compared with unhealthy NHPs). In the same animal, BAT was significantly more perfused in the supraclavicular region than in the axillary region, suggesting that axillary BAT may be the first to undergo WAT conversion as metabolism transitions from healthy to prediabetes.

Anatomical distribution of BAT

When analyzing the entire cohort of vervet monkeys, the most prominent location of BAT was identified in the supraclavicular region. The supraclavicular fossa is bounded inferiorly by the supraspinatus muscle, posteriorly by the trapezius, superolaterally by the atlantoscapularis anterior, and superomedially by the scalene muscles and

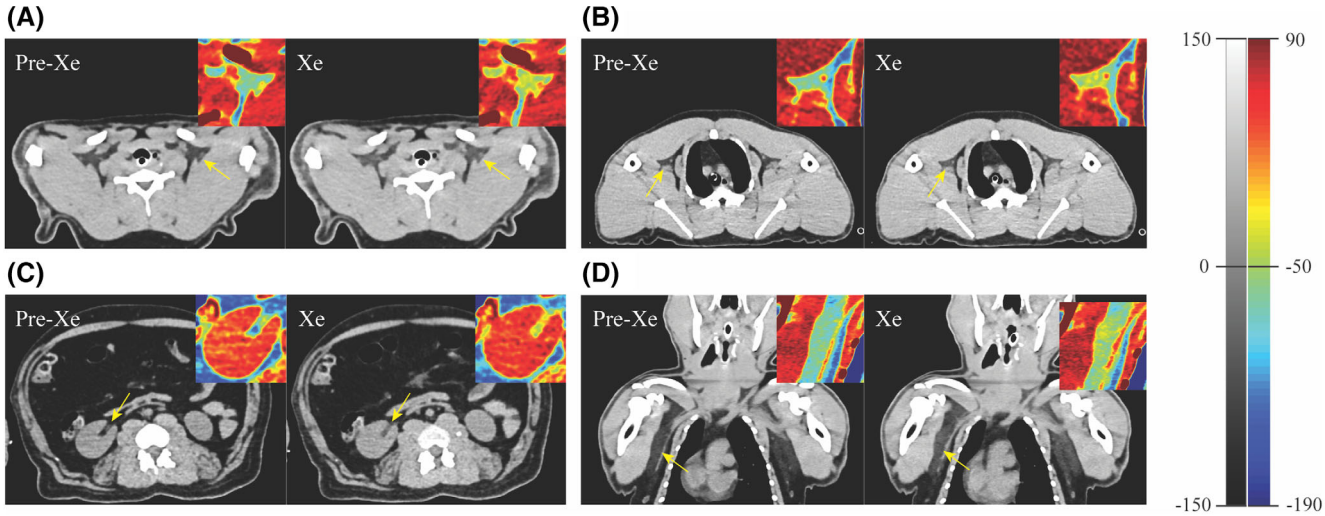

FIGURE 1 Radiodensity enhancement observed in computed tomography images during xenon inhalation and norepinephrine infusion in the (A) supraclavicular, (B,D) axillary, and (C) renal hilum regions of a lean healthy rhesus macaque [Color figure can be viewed at wileyonlinelibrary.com]

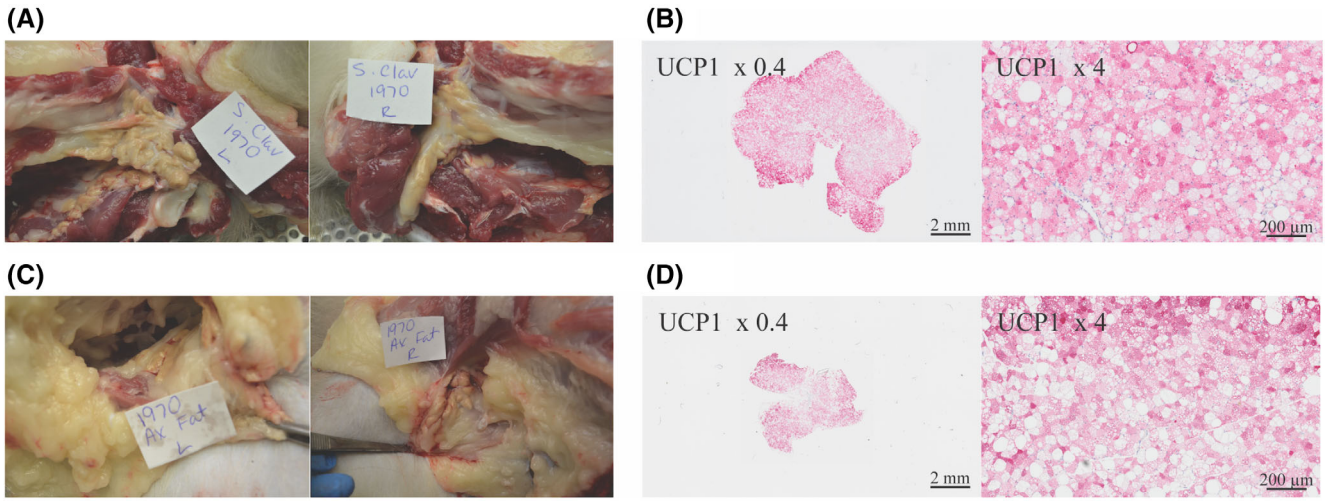

FIGURE 2 Widespread supraclavicular BAT observed on XECT (Figure 1) visualized during (A) necropsy and (B) confirmed by histology with UCP1 staining. Large axillary BAT pockets seen on XECT in the same rhesus macaque were confirmed at (C) necropsy and (D) by UCP1 staining. BAT, brown adipose tissue; UCP1, uncoupling protein 1; XECT, xenon-enhanced computed tomography [Color figure can be viewed at wileyonlinelibrary.com]

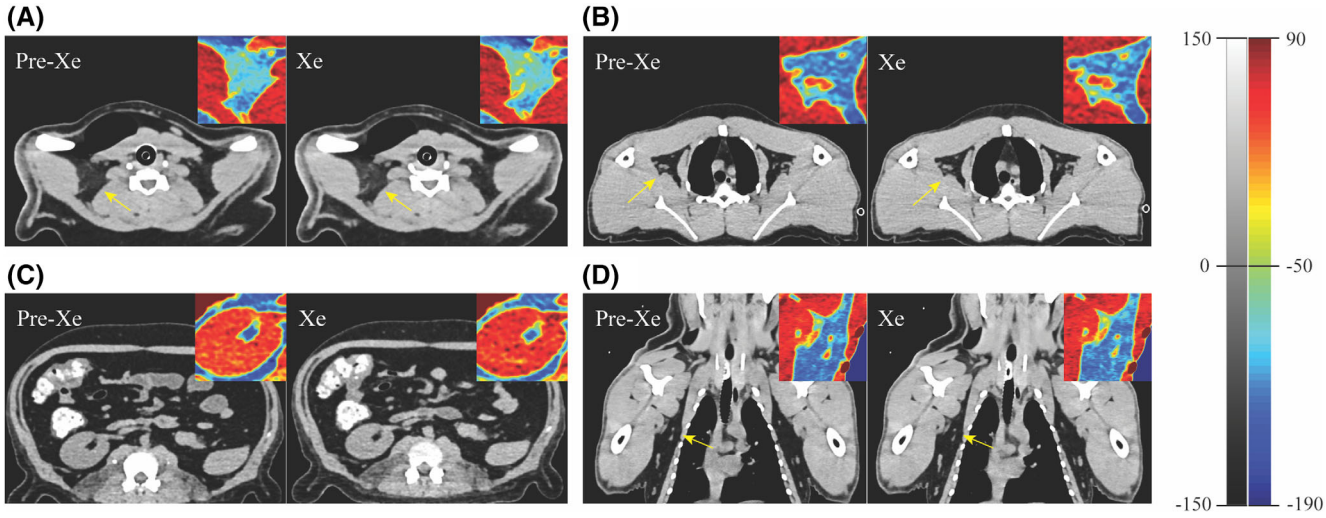

FIGURE 3 (A) Large areas of radiodensity enhancement observed on CT images during norepinephrine infusion and xenon inhalation in the supraclavicular region of a prediabetic rhesus macaque. (B,D) Limited axillary radiodensity enhancement was seen on XECT of the same rhesus macaque, and (C) no enhancement in the renal hilum was observed. CT, computed tomography; XECT, xenon-enhanced computed tomography [Color figure can be viewed at wileyonlinelibrary.com]

the atlanto-scapularis posterior. The transverse cervical artery is the most significant vascular structure in this region, originating from the thyrocervical trunk, a branch of the subclavian artery, and traveling posteriorly toward the trapezius muscle. In some healthy primates, BAT was found to be diffuse throughout the entire fat pocket (Figure 5A). In healthy obese primates, BAT was diffuse around the transverse cervical artery and its branches but was not as prevalent throughout the entire region (Figure 5B). In prediabetic and diabetic subjects, BAT existed in small pockets confined near the transverse cervical artery and its branches (Figure 5C).

More inferiorly, we identified BAT in the infraclavicular fossa of the NHPs. This region is posteroinferior to the clavicle and medial to the coracoid process of the scapula. Here, the thoracoacromial artery branches from the axillary artery. BAT in the infraclavicular fossa mimicked the same patterns as the supraclavicular fossa. In healthy subjects, BAT was diffuse throughout the entire region or diffuse in proximity to the vasculature of the region. In unhealthy subjects, BAT was limited to small pockets adjacent to the thoracoacromial artery and its branches.

The axillary fossa is another region of significant BAT presence. It is bordered medially by the thoracic wall and the serratus anterior muscle; anteriorly by the pectoralis major and minor; inferiorly by the subscapularis, teres major, and latissimus dorsi; and laterally by the long head of the biceps brachii. The axillary artery runs along the lateral edge of the region. The lateral thoracic artery travels through the

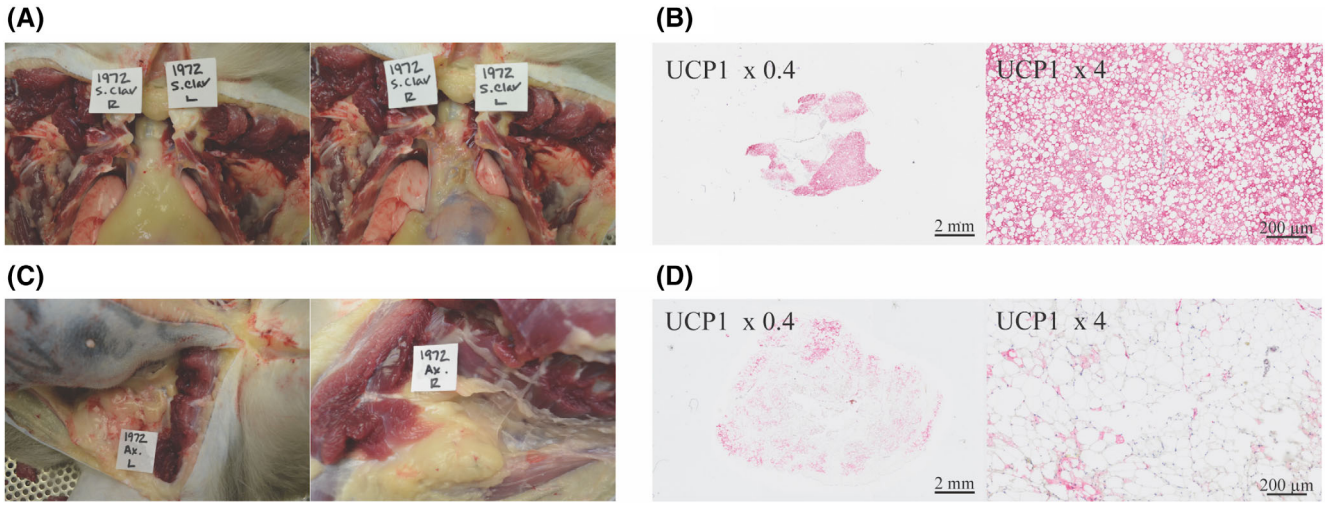

FIGURE 4 Pockets of supraclavicular BAT seen on XECT of a prediabetic rhesus macaque (Figure 3) were visualized during (A) necropsy and confirmed on (B) histology with UCP1 staining. Limited axillary radiodensity enhancement on XECT of the same rhesus macaque (Figure 3) was consistent with little BAT observation during (C) necropsy and histology with (D) UCP1 staining. BAT, brown adipose tissue; UCP1, uncoupling protein 1; XECT, xenon-enhanced computed tomography [Color figure can be viewed at wileyonlinelibrary.com]

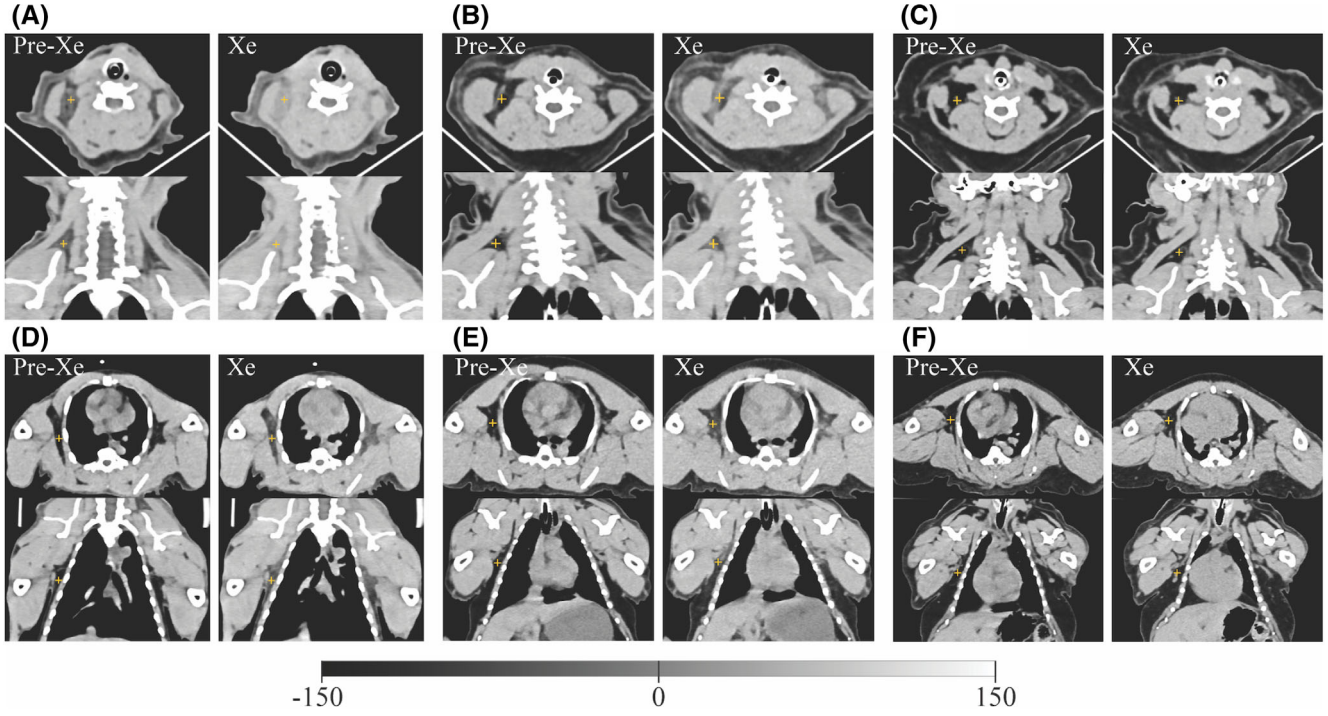

FIGURE 5 Representative differences in radiodensity enhancement observed in the supraclavicular region during norepinephrine infusion and xenon inhalation between (A) healthy lean vervet monkey (NHP 1080), (B) healthy obese vervet monkey (NHP 1299), and (C) diabetic vervet monkey (NHP 1242). Images on the left were acquired before xenon inhalation. Images on the right were acquired during xenon inhalation. Representative images showing the difference in radiodensity enhancement observed in the axillary region of (D) healthy lean vervet monkey (NHP 1080), (E) healthy obese vervet monkey (NHP 1299), and (F) diabetic vervet monkey (NHP 1242) before (left) and during (right) xenon inhalation. Intensity scale for all figures ranges from −150HU to +150 HU. NHP, nonhuman primate [Color figure can be viewed at wileyonlinelibrary.com]

anterior half of the fat pocket, and the thoracodorsal artery travels through the posterior half of the fatty pocket. Axillary BAT in healthy subjects was diffuse around the lateral thoracic and thoracodorsal arteries or confined to smaller pockets adjacent to these major arteries (Figure 5D,E). Unlike in the supraclavicular region, BAT was not as diffuse throughout the entire region. In unhealthy subjects, BAT existed in very small pockets concentrated around the major arteries and, in some subjects, almost none was present (Figure 5F).

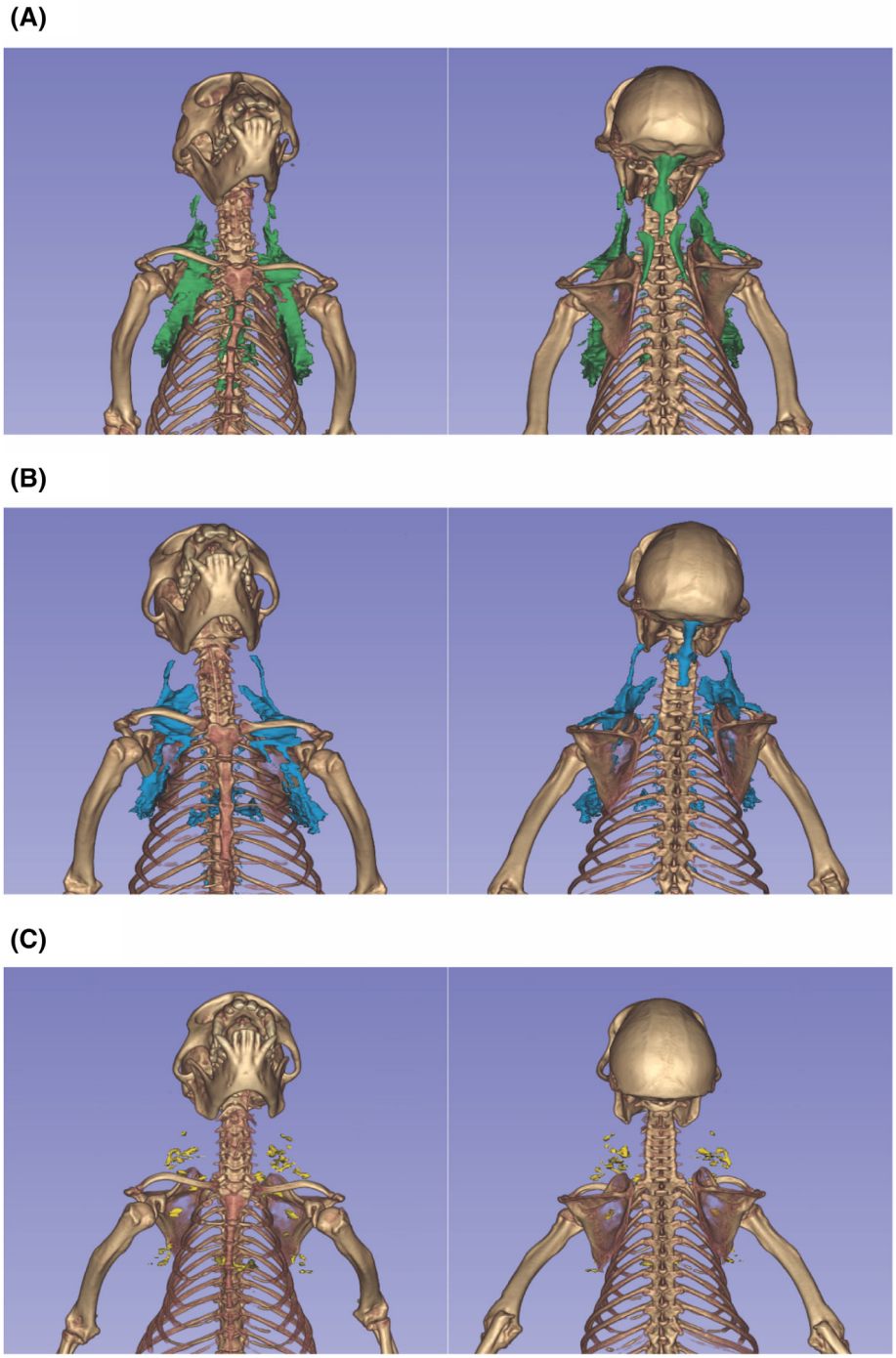

FIGURE 6 Three-dimensional segmentation of brown adipose tissue depots identified using xenon-enhanced computed tomography in (A) healthy lean vervet monkey (NHP 1080), (B) healthy obese vervet monkey (NHP 1299), and (C) diabetic vervet monkey (NHP 1242). NHP, nonhuman primate [Color figure can be viewed at wileyonlinelibrary.com]

We also identified smaller BAT depots in the cervical, paravertebral, and pericardial adipose tissue of all vervet monkeys. We found cervical BAT to lie just superior to the supraclavicular fat and that it was generally continuous with supraclavicular BAT in healthy animals. In prediabetic and diabetic vervets, the cervical BAT presented as its own smaller, discrete depot. Paravertebral BAT was most prevalent between transverse processes of the thoracic vertebrae, and pericardial BAT was most concentrated in the coronary sulcus. BAT in these regions was significantly more diffuse in healthy subjects than in unhealthy subjects (Figure 6).

In most vervet monkeys, we identified small BAT depots in the perirenal, paraspinal, and interscapular fat. In all animals, except for one diabetic vervet, we identified BAT in the perirenal adipose tissue, which was most significant around the renal hilum. In all animals, except for one diabetic vervet, we identified BAT in the paraspinal fat pad, and we identified BAT in the interscapular fat of all animals

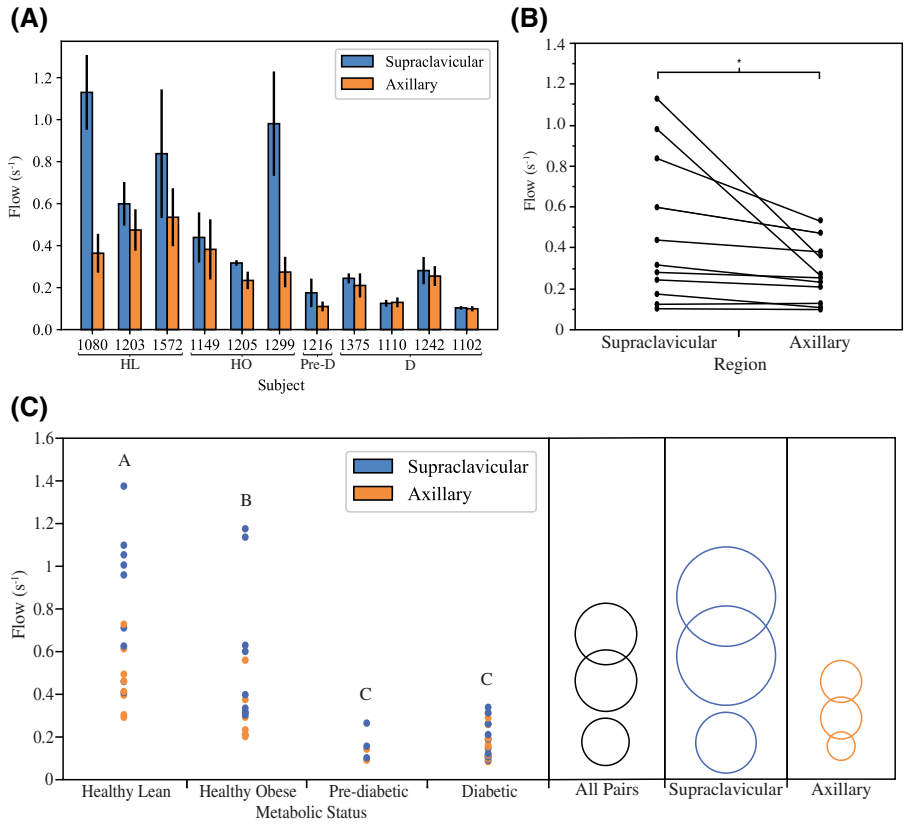

FIGURE 7 (A) Mean BAT perfusion calculated in selected regions of interest in the supraclavicular and axillary regions of HL ($n = 3$), HO ($n = 3$), Pre-D ($n = 1$), and D ($n = 4$) vervet monkeys. Three ROIs were taken from each of the two anatomical regions of each animal for a total of $n = 6$ ROIs from each vervet monkey. Error bars represent SD. (B) Mean BAT perfusion in selected regions of interest of the supraclavicular and axillary regions of each vervet monkey ($n = 11$). Connected points correspond to the same subject. A matched-pairs t test revealed significantly greater perfusion in supraclavicular BAT compared with axillary BAT (mean difference ± SE of 0.20 ± 0.06 s^{-1}, $p = 0.0009$). (C) BAT perfusion calculated in selected ROIs in the supraclavicular (blue) and axillary (orange) regions of HL ($n = 3$), HO ($n = 3$), Pre-D ($n = 1$), and D ($n = 4$) vervet monkeys. A Tukey–Kramer honestly significant difference test for multiple comparisons demonstrated significantly greater flow in HL primates than in HO ($p = 0.0160$) and unhealthy (Pre-D and D) primates ($p < 0.0001$). Additionally, significantly greater blood flow was detected in HO primates than unhealthy primates ($p = 0.0008$). BAT, brown adipose tissue; D, diabetic; HL, healthy lean; HO, healthy obese; Pre-D, prediabetic; ROI, region of interest [Color figure can be viewed at wileyonlinelibrary.com]

except for two diabetic animals. However, just as we observed with all the aforementioned depots, BAT in these regions was more widespread in healthy animals than in unhealthy animals (Figure 6).

XECT was also used to quantify volumes of the cervical, supraclavicular, axillary, and renal BAT depots in each of the 11 vervet monkeys as well as the percentage of total body fat these depots comprised (Supporting Information Table S2). Despite the low sample size and high intragroup variability, we found significantly different BAT volumes in the cervical depot of healthy lean NHPs compared with unhealthy obese NHPs, the cervical depot of healthy obese NHPs compared with unhealthy obese NHPs, and the supraclavicular depot of healthy obese NHPs compared with unhealthy obese NHPs (Supporting Information Table S3). The data also showed significantly different BAT volumes as a percentage of total body fat between all metabolic groups in the cervical depot and between healthy obese NHPs and unhealthy obese NHPs in all other depots (Supporting Information Table S3).

Differences in BAT perfusion between lean, obese, and diabetic monkeys

Measurements of BAT blood flow in the supraclavicular and axillary region of 11 vervet monkeys by XECT revealed clear differences between animals of different metabolic statuses (Figure 7A). BAT blood flow was significantly greater in healthy lean animals ($Flow_{mean}$ [SD] of 0.66 [0.32]) than in healthy obese animals ($Flow_{mean}$ [SD] of 0.44 [0.29], $p = 0.0160$) and unhealthy obese animals ($Flow_{mean}$ [SD] of 0.17 [0.08], $p < 0.0001$). BAT blood flow was also significantly greater in healthy obese animals than unhealthy obese animals ($p = 0.0008$).

Interestingly, when looking at the supraclavicular region alone, there was no significant difference in blood flow between healthy lean ($Flow_{mean}$ [SD] of 0.86 [0.33]) and healthy obese animals ($Flow_{mean}$ [SD] of 0.58 [0.35], $p = 0.0675$). However, we did find significantly greater flow in the supraclavicular region of healthy lean animals

compared with unhealthy animals ($Flow_{mean}$ [SD] of 0.19 [0.08], $p < 0.0001$) and healthy obese animals compared with unhealthy animals ($p = 0.0024$). On the other hand, when looking at just the axillary region, we found significantly greater flow in healthy lean primates ($Flow_{mean}$ [SD] of 0.46 [0.14]) compared with healthy obese primates ($Flow_{mean}$ [SD] of 0.30 [0.12], $p = 0.0099$) and unhealthy obese primates ($Flow_{mean}$ [SD] of 0.16 [0.07], $p < 0.0001$). Additionally, there was significantly greater BAT blood flow found in healthy obese animals compared with unhealthy animals ($p = 0.015$). Together these results suggest that, as the NHPs' metabolic health worsens, the BAT in the axillary region may be the first to undergo significant conversion to WAT. Despite these healthy obese primates having significantly less BAT perfusion in the axillary region compared with healthy lean primates, they did not yet show significantly less BAT perfusion in the supraclavicular region, even though BAT was notably less perfused on average. On the contrary, the healthy obese NHPs had already lost a significant amount of perfusion in the axillary region compared with the healthy lean primates. This is consistent with our 3D BAT distribution mapping of the NHPs that show similar supraclavicular distribution of BAT between healthy lean NHPs and healthy obese NHPs but notably less diffuse axillary BAT in the same healthy lean NHPs compared with the healthy obese NHPs (Figure 6).

In addition, a matched-pairs t test across all subjects demonstrated significantly greater perfusion in supraclavicular BAT than in axillary BAT (mean difference $\pm$ SE of 0.20 ± 0.06 s^{-1}, $p = 0.0009$; Figure 7B). Despite these differences, no significant differences in BAT radiodensity ($p > 0.05$ for all pairs), known to be directly correlated to tissue hydration [37], were found between healthy lean (HU_{mean} [SD] of -78 [35]), healthy obese (HU_{mean} [SD] of -95 [37]), and unhealthy obese (HU_{mean} [SD] of -95 [29]; Supporting Information Figure S6).

DISCUSSION

Understanding BAT distribution and how it changes with metabolic disease is essential for the development of therapies that aim at augmenting BAT mass and/or function. Here, by using XECT scanning, we assess differences in BAT distribution and perfusion between lean, obese, and diabetic NHP animal models. By using XECT, we were able to identify all BAT pockets within the supraclavicular and axillary depots despite the sparsity of this tissue in obese and diabetic NHPs. Although BAT and WAT had similar fat content, the increase in BAT perfusion during adrenergic stimulation of NST ultimately led to a specific radiodensity enhancement of BAT during xenon inhalation and to its detection in CT scans. Histological verification of tissue taken at necropsy confirmed that enhanced area did correspond to BAT-positive region.

Our results are consistent with a previous study that examined BAT enhancement and distribution using XECT [26], and the perfusion results are consistent with previous studies demonstrating decreased BAT activity in human subjects with obesity and diabetes [38, 39]. BAT perfusion measurements in this study unequivocally show that obesity leads to a reduction in both BAT volume and perfusion. Although we only studied one prediabetic NHP, the striking similarity in perfusion between the prediabetic subject and the diabetic subjects suggests that this decrease takes place before the onset of diabetes, and the significantly higher perfusion in healthy lean individuals compared with healthy obese individuals indicates that the decrease in perfusion begins to occur even before an individual reaches an unhealthy metabolic state.

Differences in tissue perfusion were noted not only between healthy obese subjects and diabetic subjects, but also between axillary and supraclavicular BAT. Examining the group of vervets and rhesus macaques as a whole reinforces our key findings about how supraclavicular and axillary BAT distribution changes as these NHPs naturally develop metabolic disease. We observed that, as the animals display the range of a healthy to an unhealthy metabolic status, the renal hilum and the axillary BAT depots are the first to show significant conversion to WAT, followed by the supraclavicular BAT depot. This is evident in the two-dimensional and 3D images of the vervet monkeys (Figure 5), in which the healthy lean animal showed diffuse BAT in the supraclavicular and axillary regions and the healthy obese animal showed diffuse BAT in the supraclavicular region but decreased BAT mass in the axillary region. Although the diabetic vervet in these images showed limited BAT mass in general, it is still notable that more supraclavicular BAT mass is present than axillary BAT mass. The same pattern was observed in the rhesus. The healthy lean rhesus showed diffuse supraclavicular and axillary BAT on XECT that was confirmed through necropsy and histology. The prediabetic rhesus, which has not yet progressed to overt diabetes, still shows large amounts of supraclavicular BAT mass but shows a sparse distribution of axillary BAT on XECT that was also evident at necropsy in the gross and immunohistochemical images. Interestingly, together these findings are consistent with the reduced incidence in axillary BAT observed in adult humans, again suggesting similar differences in BAT distribution and perfusion between NHPs and humans.

Interestingly, despite the clear differences in BAT perfusion among vervet monkeys of varying metabolic statuses, no significant differences were seen in tissue radiodensity, used here as a proxy for tissue's hydration. Indeed, in CT images fat tissue radiodensity is, by and large, determined by the relative concentration of water and fat molecules in the tissue. BAT radiodensity, in particular, has already been used as an indication of tissue hydration [37] and as a way of measuring changes in tissue hydration following cold exposure [17, 40]. The absence of clear differences in BAT radiodensity between the three different groups reinforces the notion that BAT presence and activity cannot be determined based on tissue hydration and fat content alone (Supporting Information Figures S6-S7) [18, 27, 28].

It is important to note that detection of BAT mass by XECT relies on two key elements: the high solubility of xenon in fat and the selective enhancement in blood flow to BAT during stimulation of NST. The latter, although it can certainly provide a qualitative indication of the ability of the tissue to sustain the increased oxygen demand during thermogenesis, cannot be used as a proxy for thermogenic activity [41].

Although XECT is already used clinically for studying lung ventilation and brain perfusion [20–22], it does have limitations. First, the radiation dose associated with repeated CT scans may prevent the use of XECT for repeated BAT blood flow measurements in humans. Second, although the inhalation of 28% xenon is safe, with minimal risks and side effects that are quickly reversible [42], at doses greater than 28%, xenon may lead to more frequent and unwanted side effects, which include respiratory suppression, hyperventilation, nausea/vomiting, anxiety, hypertension, and numbness [42].

CONCLUSION

Here, we demonstrated that XECT is an accurate tool to identify BAT within the much larger WAT depot and to examine its distribution, morphology, and perfusion. By using XECT, we were able to identify small BAT pockets within the much larger supraclavicular and axillary adipose depots of lean, obese, and diabetic NHPs. By using dynamic XECT scanning, we found BAT perfusion to be independent of its fat content and, along with its distribution, to be directly correlated to the metabolic status of the animal. Given the strong similarity between humans and NHPs, similar differences in BAT distribution and perfusion may be expected in humans.O

AUTHOR CONTRIBUTIONS

Rosa T. Branca had full access to all the data in the study and takes responsibility for the integrity of the data and the accuracy of the data analysis. Study concept and design: Rosa T. Branca and Kylie Kavanagh; analysis and interpretation of data: John C. Garside, Rosa T. Branca, and Kylie Kavanagh; data collection and management: Rosa T. Branca, Kylie Kavanagh, Masha R. Block, and Abigail G. Williams; drafting of the manuscript: John C. Garside, Rosa T. Branca, and Kylie Kavanagh.

ACKNOWLEDGMENTS

This study includes imaging and immunohistochemical digital data, which will be made available upon request.

FUNDING INFORMATION

This work was supported by the National Institute of Diabetes and Digestive and Kidney Diseases (NIDDK) through grant No. R01DK108231 and R01DK123206 (to RTB), by the National Institute of Health through grant No. ULTR001420, P40OD010954, P40OD010965, and R01HL142930, and by the Assistant Secretary of Defense for Health Affairs endorsed by the Department of Defense, through the Peer Reviewed Medical Research Program under Award No. W81XWH1510574 and W81XWH2110565 (to RTB). Opinions, interpretations, conclusions and recommendations are those of the authors and are not necessarily endorsed by the Department of Defense.

CONFLICT OF INTEREST

The authors declared no conflict of interest.

ORCID

John C. Garside https://orcid.org/0000-0001-8917-5007
Kylie Kavanagh https://orcid.org/0000-0001-8772-6186
Rosa T. Branca https://orcid.org/0000-0002-6871-1824

REFERENCES

1. Jastroch M, Wuertz S, Kloas W, Klingenspor M. Uncoupling protein 1 in fish uncovers an ancient evolutionary history of mammalian nonshivering thermogenesis. *Physiol Genomics*. 2005;22:150-156.
2. Cannon B, Nedergaard J. The biochemistry of an inefficient tissue: brown adipose tissue. *Essays Biochem*. 1985;20:110-164.
3. Cannon B, Nedergaard J. Brown adipose tissue: function and physiological significance. *Physiol Rev*. 2004;84:277-359.
4. Krauss S, Zhang CY, Lowell BB. The mitochondrial uncoupling-protein homologues. *Nat Rev Mol Cell Biol*. 2005;6:248-261.
5. Leitner BP, Huang S, Brychta RJ, et al. Mapping of human brown adipose tissue in lean and obese young men. *Proc Natl Acad Sci USA* 2017;114:8649-8654.
6. Cypess AM, Haft CR, Laughlin MR, Hu HH. Brown fat in humans: consensus points and experimental guidelines. *Cell Metab*. 2014;20:408-415.
7. Sampath SC, Sampath SC, Bredella MA, Cypess AM, Torriani M. Imaging of brown adipose tissue: state of the art. *Radiology*. 2016;280:4-19.
8. Ouellet V, Routhier-Labadie A, Bellemare W, et al. Outdoor temperature, age, sex, body mass index, and diabetic status determine the prevalence, mass, and glucose-uptake activity of 18F-FDG-detected BAT in humans. *J Clin Endocrinol Metab*. 2011;96:192-199.
9. Hankir MK, Kranz M, Keipert S, et al. Dissociation between brown adipose tissue 18F-FDG uptake and thermogenesis in uncoupling protein 1-deficient mice. *J Nucl Med* 2017;58:1100-1103.
10. Olsen JM, Csikasz RI, Dehvari N, et al. β3-Adrenergically induced glucose uptake in brown adipose tissue is independent of UCP1 presence or activity: mediation through the mTOR pathway. *Mol Metab*. 2017;6:611-619.
11. Orava J, Nuutila P, Lidell ME, et al. Different metabolic responses of human brown adipose tissue to activation by cold and insulin. *Cell Metab* 2011;14:272-279.
12. van der Lans AAJJ, Wierts R, Vosselman MJ, Schrauwen P, Brans B, van Marken Lichtenbelt WD. Cold-activated brown adipose tissue in human adults: methodological issues. *Am J Physiol Regul Integr Comp Physiol*. 2014;307:R103-R113.
13. van Marken Lichtenbelt WD, Vanhommerig JW, et al. Cold-activated Brown adipose tissue in healthy men. *N Engl J Med* 2009;360:1500-1508.
14. McHugh CT, Garside J, Barkes J, et al. Differences in [18F]FDG uptake in BAT of UCP1−/− and UCP1+/+ during adrenergic stimulation of non-shivering thermogenesis. *EJNMMI Res*. 2020;10:136. doi:10.1186/s13550-020-00726-x
15. Hu HH, Smith DL, Nayak KS, Goran MI, Nagy TR. Identification of brown adipose tissue in mice with fat-water IDEAL-MRI. *J Magn Reson Imaging*. 2010;31:1195-1202.
16. Lubura M, Hesse D, Neumann N, Scherneck S, Wiedmer P, Schürmann A. Non-invasive quantification of white and brown adipose tissues and liver fat content by computed tomography in mice. *PLoS ONE* 2012;7:e37026. doi:10.1371/journal.pone.0037026
17. Baba S, Jacene HA, Engles JM, Honda H, Wahl RL. CT Hounsfield units of brown adipose tissue increase with activation: preclinical and clinical studies. *J Nucl Med*. 2010;51:246-250.
18. Branca RT, Zhang L, Warren WS, et al. In vivo noninvasive detection of Brown adipose tissue through intermolecular zero-quantum MRI. *PLoS ONE* 2013;8:e74206. doi:10.1371/journal.pone.0074206
19. Branca RT, He T, Zhang L, et al. Detection of brown adipose tissue and thermogenic activity in mice by hyperpolarized xenon MRI. *Proc Natl Acad Sci USA*. 2014;111:18001-18006.

20. Bouma GJ, Muizelaar JP, Stringer WA, Choi SC, Fatouros P, Young HF. Ultra-early evaluation of regional cerebral blood flow in severely head- injured patients using xenon-enhanced computerized tomography. *J Neurosurg*. 1992;77:360-368.
21. Vedantam A, Robertson CS, Gopinath SP. Quantitative cerebral blood flow using xenon-enhanced CT after decompressive craniectomy in traumatic brain injury. *J Neurosurg*. 2018;129:241-246.
22. Good WF, Gur D. Xenon-enhanced CT of the brain: effect of flow activation on derived cerebral blood flow measurements. *AJNR Am J Neuroradiol*. 1991;12:83-85.
23. SS K. The theory and applications of the exchange of inert gas at the lungs. *Pharmacol Rev*. 1951;3:59-106.
24. Wintermark M, Thiran JP, Maeder P, Schnyder P, Meuli R. Simultaneous measurement of regional cerebral blood flow by perfusion CT and stable xenon CT: a validation study. *AJNR Am J Neuroradiol*. 2001;22:905-914.
25. Joseph M, Nates J. Stable xenon computed tomography cerebral blood flow measurement in neurological disease: review and protocols. *The Internet Journal of Emergency and Intensive Care Medicine*. 1999;4:2. http://ispub.com/IJEICM/4/2/4567
26. Branca RT, McCallister A, Yuan H, et al. Accurate quantification of brown adipose tissue mass by xenon-enhanced computed tomography. *Proc Natl Acad Sci USA* 2018;115:174-179.
27. Foster DO, Frydman ML. Tissue distribution of cold-induced thermogenesis in conscious warm- or cold-acclimated rats reevaluated from changes in tissue blood flow: the dominant role of brown adipose tissue in the replacement of shivering by nonshivering thermogenesis. *Can J Physiol Pharmacol*. 1979;57:257-270.
28. Muzik O, Mangner TJ, Leonard WR, Kumar A, Janisse J, Granneman JG. 15O PET measurement of blood flow and oxygen consumption in cold-activated human brown fat. *J Nucl Med*. 2013;54:523-531.
29. Kavanagh K, Davis AT, Peters DE, LeGrand AC, Bharadwaj MS, Molina AJA. Regulators of mitochondrial quality control differ in subcutaneous fat of metabolically healthy and unhealthy obese monkeys. *Obesity (Silver Spring)*. 2017;25:689-696.
30. Swick AG, Kemnitz JW, Houser WD, Swick RW. Norepinephrine stimulates activity of brown adipose tissue in rhesus monkeys. *Int J Obes*. 1986;10:241-244.
31. Walston J, Lowe A, Silver K, et al. The β3-adrenergic receptor in the obesity and diabetes prone rhesus monkey is very similar to human and contains arginine at codon 64. *Gene* 1997;188:207-213.
32. Fisher MH, Amend AM, Bach TJ, et al. A selective human β3 adrenergic receptor agonist increases metabolic rate in rhesus monkeys. *J Clin Invest* 1998;101:2387-2393.
33. Fedorov A, Beichel R, Kalpathy-Cramer J, et al. 3D slicer as an image computing platform for the quantitative imaging network. *Magn Reson Imaging* 2012;30:1323-1341.
34. Drayer BP, Wolfson SK, Reinmuth OM, Dujovny M, Boehnke M, Cook EE. Xenon enhanced CT for analysis of cerebral integrity, perfusion, and blood flow. *Stroke*. 1978;9:123-130.
35. Yonas H, Gur D, Wolfson SK, Good WF, Good BC, Latchaw RE. Xenon-enhanced computerised tomographic cerebral blood flow mapping. *Lancet*. 1984;1:1357. doi:10.1016/s0140-6736(84)91856-7
36. Yonas H, Pindazola RR, Johnson DW. Xenon/computed tomography cerebral blood flow and its use in clinical management. *Neurosurg Clin N Am*. 1996;7:605-616.
37. Din MU, Raiko J, Saari T, et al. Human brown fat radiodensity indicates underlying tissue composition and systemic metabolic health. *J Clin Endocrinol Metab*. 2017;102:2258-2267.
38. Vijgen GHEJ, Bouvy ND, Teule GJJ, Brans B, Schrauwen P, van Marken Lichtenbelt WD. Brown adipose tissue in morbidly obese subjects. *PLoS ONE*. 2011;6:e17247. doi:10.1371/journal.pone.0017247
39. Vijgen GHEJ, Bouvy ND, Teule GJJ, et al. Increase in brown adipose tissue activity after weight loss in morbidly obese subjects. *J Clin Endocrinol Metabol* 2012;97:E1229-E1233.
40. Blondin DP, Labbé SM, Phoenix S, et al. Contributions of white and brown adipose tissues and skeletal muscles to acute cold-induced metabolic responses in healthy men. *J Physiol* 2015;593:701-714.
41. Abreu-Vieira G, Hagberg CE, Spalding KL, Cannon B, Nedergaard J. Adrenergically stimulated blood flow in brown adipose tissue is not dependent on thermogenesis. *Am J Physiol Endocrinol Metab*. 2015;308:E822-E829.
42. Carlson AP, Brown AM, Zager E, et al. Xenon-enhanced cerebral blood flow at 28% xenon provides uniquely safe access to quantitative, clinically useful cerebral blood flow information: a multicenter study. *Am J Neuroradiol* 2011;32:1315-1320.

SUPPORTING INFORMATION

Additional supporting information can be found online in the Supporting Information section at the end of this article.

How to cite this article: Garside JC, Kavanagh K, Block MR, Williams AG, Branca RT. Xenon-enhanced computed tomography assessment of brown adipose tissue distribution and perfusion in lean, obese, and diabetic primates. *Obesity (Silver Spring)*. 2022;30(9):1831-1841. doi:10.1002/oby.23519